COMPARISON OF WATER BOILING MODELS AGAINST RECENT EXPERIMENTAL DATA, WITH SPECIAL EMPHASIS ON THE BUBBLE EBULLITION CYCLE

By

Matthew Miguel Virgen

SUBMITTED TO THE DEPARTMENT OF NUCLEAR SCIENCE AND ENGINEERING IN PARTIAL FULLFILLMENT OF THE REQUIREMENTS FOR THE DEGREE OF

BACHELOR OF SCIENCE IN NUCLEAR SCIENCE AND ENGINEERING   **ARCHIVES**
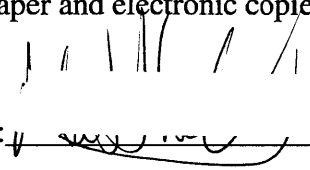
AT THE

MASSACHUSETTS INSTITUTE OF TECHNOLOGY

JUNE 2011

Matthew Miguel Virgen. All Rights Reserved

The author hereby grants to MIT permission to reproduce and to distribute publicly

Paper and electronic copies of this thesis in whole or in part.

Signature of Author:_____

<div align="right">

Matthew Miguel Virgen

Department of Nuclear Science and Engineering

May 19 2011

</div>

Certified by:_____

<div align="right">

Jacopo Buongiorno - Thesis Supervisor

Associate Professor of Nuclear Science and Engineering

</div>

Certified by:_____

<div align="right">

Michael Z. Podowski – Thesis Co-Supervisor

Visiting Professor

</div>

Accepted by:_____

<div align="right">

Dennis Whyte

Professor of Nuclear Science and Engineering

Chairman, NSE Committee for Undergraduate Students

</div>

1

COMPARISON OF WATER BOILING MODELS AGAINST RECENT EXPERIMENTAL DATA, WITH SPECIAL EMPHASIS ON THE EBULLITION CYCLE

By

Matthew Miguel Virgen

Submitted to the Department of Nuclear Science and Engineering on May 19, 2011

In Partial Fulfillment of the Requirements for the Degree of

Bachelor of Science in Nuclear Science and Engineering

ABSTRACT

Using recently collected data which was measured with state-of-the-art techniques, models for nucleation site density, bubble departure diameter, and nucleation frequency were compared against the acquired data. The particular focus of this work is on the ebullition cycle and associated bubble nucleation frequency, looking at the models proposed by M.Z. Podowski. In my analysis, I took the average values for the growth and dwell times directly from the data, rather than from the models for those parameters. The results of those investigations showed that the basic principles approach for considering the parameters of the ebullition cycle held up pretty well with the experimental data, with $T_i(t)$, the temperature curve during the ebullition cycle, corresponding remarkably well with the data curves. However, one parameter which was always overvalued was $T(0^+)$ – the predicted temperature of the start of the dwell phase. It was generally 1-2 degrees Celsius higher than the experimental value. For a fully rigorous analysis of the ebullition models in future works, it is recommended that all parameters be predicted rather than pulled from the data, particularly of the growth and dwell times.

Thesis Supervisor: Jacopo Buongiorno

Title: Associate Professor of Nuclear Science and Engineering

Acknowledgements

Professor Jacopo Buongiorno: I would like to express my gratitude for the time you dedicated to me in helping me to understand and progress in this work. If I ever had any questions you were always ready with an insightful response, and encouraged me to continue to delve deeper into the topics. Thank you for your patience, guidance, and necessary pressure that helped me accomplish as much as I did in the small amount of time that I gave myself. It was an honor to have you as an advisor

Professor Michael Podowski: I would like to thank you as well for the time you spent with me, both at our weekly meetings and whenever I would come in with some questions. You were always ready with some feedback on my work and what direction I could take that in next. I appreciate and valued your advice on how to approach a problem and the idea of problem formulation, and I hope to be able to implement that in my professional career.

Craig Douglas Gerardi: The foundation of this work is based on the data you originally collected for your own thesis, and I want to thank you for continuing to be a support as I tried to figure out how to analyze and interpret the data. Your continued connection to your work and high willingness to help both impressed me, and I am grateful for them.

Table of Contents

List of Figures

List of Tables

Nomenclature

C	degrees celsius
c_{pf}	specific heat of the fluid
c_{pw}	specific heat of the wall
D_b	diameter of the bubble at time of departure
h_{fg}	latent heat of evaporation
k_f	thermal conductivity of the fluid
k_w	thermal conductivity of the wall
Pr	the Prandtl number
$q"$	average steady-state wall heat flux
r_c	cavity radius
T_B	liquid bulk temperature
$T_i(t)$	instantaneous wall surface temperature at nucleation site
T_o	average wall surface temperature at nucleation site during ebullition cycle
T_{sat}	saturation temperature
v_{fg}	specific volume

Greek Symbols

α_f	thermal diffusivity of the fluid
α_w	thermal diffusivity of the wall
ρ_f	density of the fluid phase
ρ_g	density of the vapor phase
σ	surface tension of the fluid
Θ_D	bubble dwell time
Θ_G	bubble growth time
μ	dynamic viscosity of the fluid

1. Introduction

The boiling phenomenon is one which is of critical importance for both nuclear systems and many engineering practices in general. This primary heat transfer mechanism lies at the heart of most power generation systems, and plays a central role in reactor physics as well.

However, trying to precisely capture the nature and characteristics of this behavior, while already studied extensively, has proved difficult to fully encapsulate in any one model or correlation, due to the fundamentally random process, as well as the large number of parameters on which boiling is dependent on. Especially now, as we develop more and more sophisticated for analyzing and predicting fluid behavior, the limiting factor is becoming the dependability and uncertainty of the models on which those calculations are based.

This work will look at various models and correlations for bubble characteristics, and then focus on some of the mechanistic models produced by Professor Mike Podowski for bubble ebullition cycle, and compare/validate them against experimental data obtained by Professor Jacopo Buongiorno.

2. Pool Boiling

The dynamics of pool boiling involves superheating the liquid which fills the micro-cavities on the heated surface, vaporizing that small amount of fluid and creating a bubble within the cavity which then expands outwards. Once the vapor forms a hemisphere atop the cavity, with a radius equal the cavity radius r_c, it then rapidly expands into the full sized bubble of diameter D_b. At that point the bubble departs from the surface, and 'cool' fluid rushes back to the surface, including the cavity, to begin the process anew.

There are three core parameters that have been associated with pool boiling, and which have been attempted to be modeled. One is the nucleation site density (NSD), which is the number of nucleation sites per unit area of the heated surface. As the heat flux increases, more cavities become active, and the NSD will increase. The other is the diameter D_b at which the bubble will depart from the surface; this is a function of various effects such as surface tension, buoyancy forces, and shear forces, and is perhaps the most difficult to model accurately.

When investigating the bubble growth at a nucleation site, there are two distinct phases. One is the period during which the liquid in the cavity is being vaporized and slowly forms a bubble within the cavity; this is called the dwell phase, and has a corresponding characteristic time called the dwell time, Θ_D. Once the vapor has reached a critical diameter, it enters the growth phase where it rapidly expands to a bubble with radius D_b; this phase has a characteristic time called the growth time, Θ_G. At the end of this phase, the cycle begins again with the dwell phase. The sum of these two consecutive phases is the ebullition cycle, which has a period equal to the sum growth and wait times. What emerges from this is the bubble nucleation frequency for a given site, with the frequency being the inverse of the period, as shown in Equation 1.

$$f = \frac{1}{\theta_D + \theta_G} \qquad (2.1)$$

As such, the primary parameters which have been measured and modeled are the bubble diameter, the nucleation site density, and the bubble nucleation frequency, which is itself a function of the growth and dwell times, as shown in Eq. 1.

3. Experiment

The experimental data is used as a reference for the validation of the various models that have

been put forth for the parameters concerning pool boiling. The experiment used state of the art

techniques in order to collect data which was as precise and detailed as possible.

3.1 Experimental Setup

High speed infrared (IR) and visible cameras simultaneously observed the heat transfer

phenomenon occurring on the heater surface. An aluminum test cell sat in an isothermal bath

equipped with an electric heater. The heating element is made of Indium-Tin-Oxide (ITO), and

was heated by passing a DC current through it, ie by Joule heating. A schematic of the pool

boiling facility can be seen in Figure 3.1
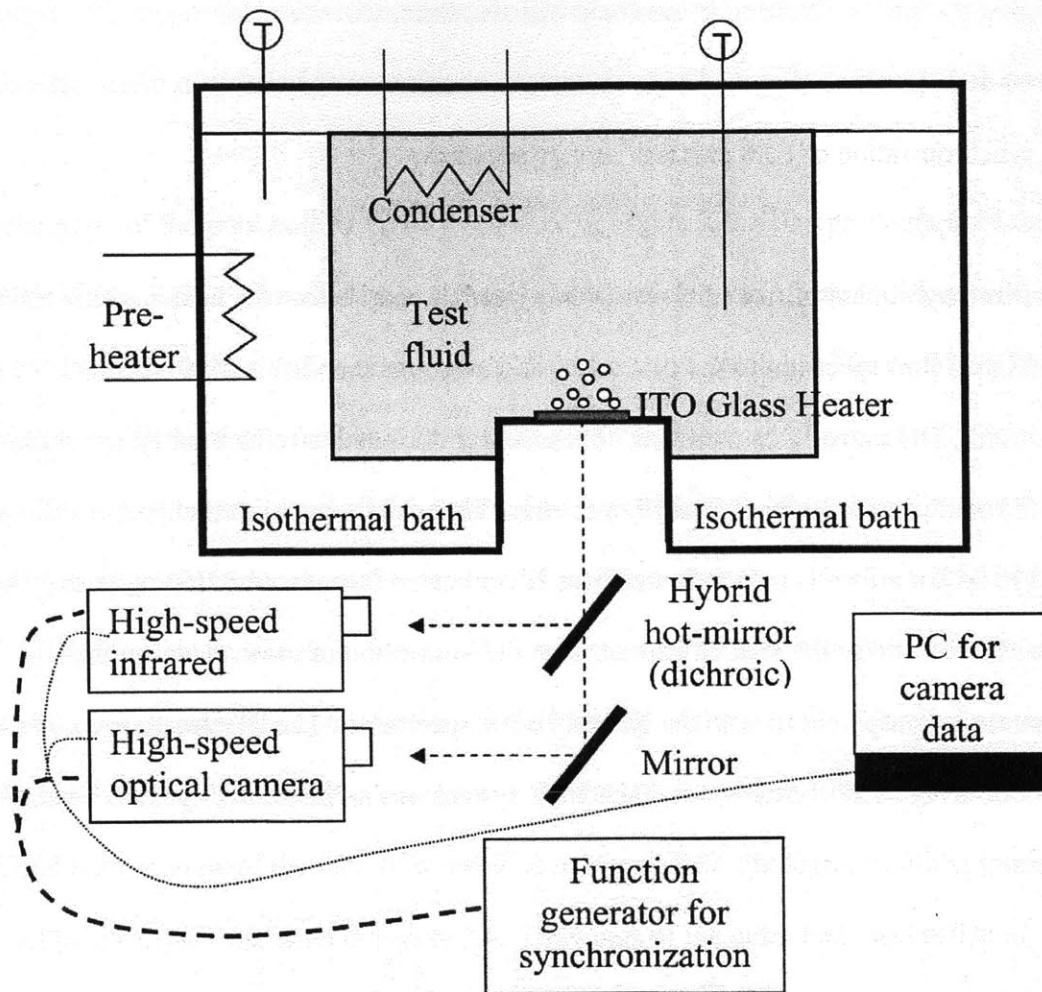
Figre 3.1: Schematic of the pool boiling facility

Boiling occurred on the upward facing side of the ITO, which had an exposed area of 30x10 mm^2, and was 0.7 μm thick. For the boiling experiments, the ITO was vacuum deposited onto a sapphire substrate which was 0.4mm thick. Due to the extreme thinness of the ITO heater, it is primarily the material properties of the sapphire which dictates heat transfer to the fluid. The material properties of the ITO and sapphire glass used in the experiments are shown in table 3.1.

Tabe 3.1: Heating element material thermal properties (T=100C)

	ρ (kg/m^3)	C_p	k
ITO	7160	340	8.7
Sapphire	3980	760	30

The basis of data collection was by using a high speed infrared (IR) camera to acquire temperature distributions across the heater surface. The IR camera used was an SC6000 from FLIR Systems, Inc. For the sake of this study, the IR camera was configured with a spatial resolution of 100µm, and a capture rate of 500 Hz, or one frame per 0.002 seconds.

3.2 Data Collection

The outer edges of the bubbles are determined by the clear contrast that occurs due to the steep temperature gradients that occur during bubble formation. A sample of a picture taken by the IR camera with a yellow line bisecting the nucleation can be seen in Figure 3.2.

Figure 3.2: Sample screenshot with a single nucleation site selected and bisected for data collection. The IR camera picks up the cold (dark) nucleation sites during the growth phase.

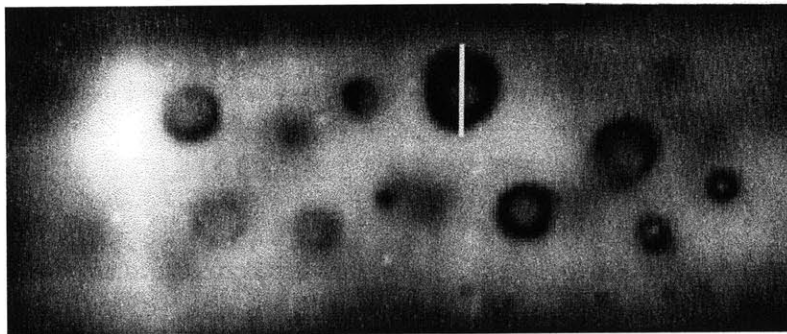The acquisition of bubble diameter data was done manually, since automated methods proved unreliable. This method consisted of selecting the outer edges of each nucleation site and drawing a line through its diameter. The uncertainty in measuring the bubble departure diameter arose from three factors: accuracy of the distance calibration, measurement bias, and not capturing the exact moment of departure. The total uncertainty arising from these three factors was found to be on the order of 10% of the bubble departure diameter.

The nucleation site density was found simply by taking the total number of nucleation sites and dividing by the total heated area. Since each of the sites were selected manually, and every frame searched for new nucleation sites, the uncertainty is expected to be negligible, <2%.

The bubble departure frequency for a given nucleation site was found by taking the peak to peak temperature response for the center pixel of each nucleation site, where this temperature response corresponds with the ebullition cycle. The growth time was found by looking at the derivative of the temperature response of the average temperature of the entire nucleation site. The start of the bubble growth time is when the average temperature at the nucleation site begins to decline, while the end of the growth time corresponded with the time at which the derivative of the temperature equaled zero. The uncertainty in the growth and wait time measurements are dictated by the frame rate, such that the absolute error could be as large as 4ms, which would correspond to missing both the start and end of the cycles by 1 frame. Depending on the length of the growth and dwell times, the uncertainty in the values also changes, but it is expected that the mean times reflect the true times well due to the large number of data points, with a maximum uncertainty of ±20%. A sample temperature response graph (ebullition cycle) can be found in Figure 3.3.
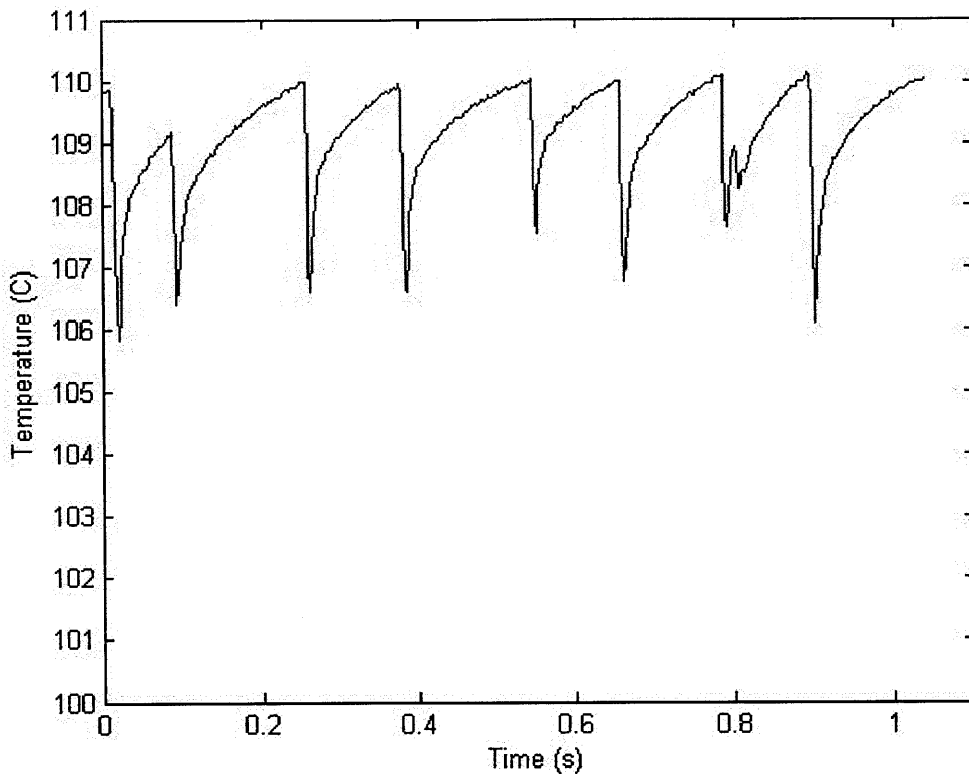
Figure 3.3: Temperature response cycle of a single nucleation site in DI Water (08_002), with the characteristic slow heating and rapid cooling cycles, corresponding with the wait and growth times, respectively.

For further details on the experiment and data collection methodology, the reader is referred to the PhD thesis by Craig Douglas Gerardi, which provides a complete description of the experiment.

4. Models

Due to its central nature in many engineering processes, the water boiling phenomenon has been studied and attempted to be understood and modeled for many years. Various different models, most of them empirical, have been proposed over time, all of them with a specific set of assumptions or data from which they are derived. In this work I compare the experimental data against some of these models, and then delve into the specifics of Professor Podowski's

14

mechanistic models for the bubble ebullition cycle and nucleation frequency. These attempt to assess the ebullition cycle from a purely theoretical standpoint, making as few assumptions as possible and accounting for all factors involved in this energy-balance problem.

A popular approach for considering heat transfer from basic principles is called heat flux partitioning, by Kurul and Podowski (1990), also called the RPI Model. The model considers three primary methods by which heat is removed by the boiling fluid, and accounts for them individually. The total boiling heat flux is obtained through the addition of the three fluxes:

$$q_{tot} = q_e + q_q + q_c \qquad (4.1)$$

In this formulation, q_e is the evaporative heat flux, which goes towards actually boiling the fluid to get the bubbles (growth phase), q_q is the quenching heat flux, which is the heat expended to heat the water which rushes in to fill the void left by the departing bubble (dwell phase), and q_c is the heat transferred to the liquid by natural convection without the influence of bubbles.

Table 4.1 contains the fluid and wall properties used for calculating the models.

Table 4.1. Wall and fluid properties

	k (W/mK)	C_p (J/kgK)	ρ (kg/m³)	μ (Pa*s)	h (J/kg)	σ (N/m)
Liquid	0.67909	4215.7	958.35	2.817e-4	419,060	0.05891
Vapor	0.02510	2080	0.598	1.227e-5	2,675,570	0.05891
Wall (sapphire)	30	760	3980	--	--	--

4.1 Bubble Diameter

The bubble diameter is the product of the net effect of all the forces acting on the bubble. Interfacial surface tension, inertial forces, buoyancy effects, and drag and lift forces in the case

15

of liquid flow, all play a role in deciding for how long the bubble grows at the site, and how large

it gets prior to departure. A few of these correlations have been used as a basis for comparing to

the experimental data. The first correlation is by Fritz (1935), which assumes that there is a

balance between surface tension and buoyancy forces at the moment of departure, with the effect

of the contact angle being taken into account empirically:

$$D_b = 0.0208\theta \left[\frac{2\sigma}{g(\rho_l - \rho_v)}\right]^{1/2} \tag{4.2}$$

Zuber (1959) developed a model that takes into account the size of the bubble relative to the

superheated boundary layer thickness:

$$D_b = \left[\frac{6k_l(T_w - T_{sat})}{q''}\right]^{1/3} \left[\frac{\sigma}{g(\rho_l - \rho_v)}\right]^{1/3} \tag{4.3}$$

Jensen and Memmel (1986) used a slightly modified version of the Kutateladze and Gorgonin

(1979) formulation, which factored in the Jakob, Prandtl, and Archimedes number:

$$D_b = 0.19(1.8 + K_1)\left[\frac{\sigma}{g(\rho_l - \rho_v)}\right]^{1/2} \tag{4.4}$$

Where K_1 is the dimensionless group:

$$K_1 = \left(\frac{Ja}{Pr_l}\right)\left(\left[\frac{g\rho_l(\rho_l - \rho_v)}{\mu_l^2}\right]\left[\frac{\sigma}{g(\rho_l - \rho_v)}\right]^{3/2}\right)^{-1} \tag{4.5}$$

Stephan (1992) also developed a correlation by modifying the Kutateladze and Gorgonin (1979)

formulation:

$$D_b = 0.25\left[1 + \left(\frac{Ja}{Pr_l}\right)^2\frac{1}{Ar}\right]^{1/2}\left[\frac{\sigma}{g(\rho_l - \rho_v)}\right]^{1/2} \; for \; 5x10^{-7} \leq \left(\frac{Ja}{Pr_l}\right)^2\frac{1}{Ar} \leq 0.1 \tag{4.6}$$

The predictions for these models for saturated water at atmospheric pressure can be seen in Figure 4.1.
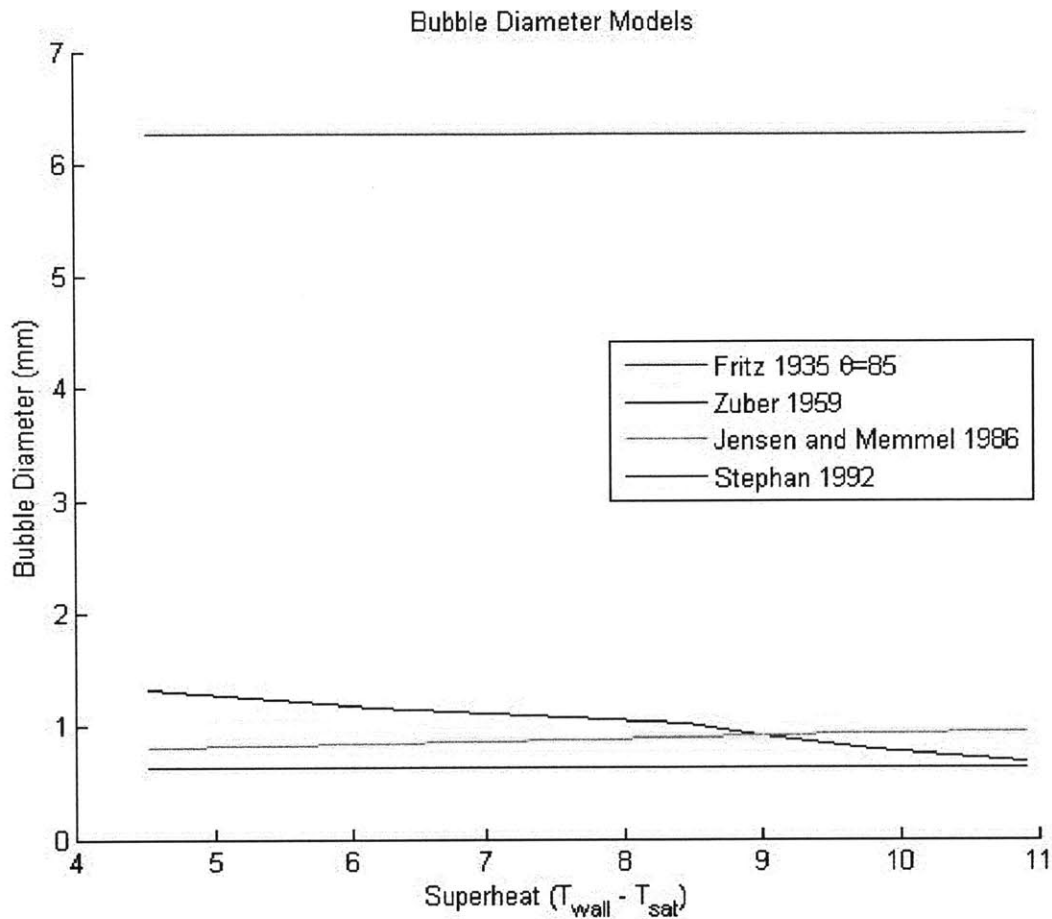
Figure 4.1: Select models of bubble diameters for saturated water at atmospheric pressure, plotted against the superheat dT.

4.2 Nucleation Site Density

For a given cavity, there is a minimum superheat necessary to activate it and create a nucleation site. As the heat flux and superheat increase, more and more of these cavities will become active, and the nucleation site density will correspondingly increase. The difficulty that lies in modeling the nucleation site density is that it requires a very precise knowledge of the nature of the heated surface. While mechanistic models have been developed for the activation of a single

17

cavity, a true mechanistic model for the nucleation site density would require knowing the details of every single cavity on the heated surface, which is plainly impractical. A general empirical formulation which has arisen for the nucleation site density can be seen in Equation 4.7, where both m and K are a function of the specifics of the boiling conditions and heater surface.

$$NSD = K\Delta T^m \tag{4.7}$$

4.3 Ebullition Cycle and Frequency

As mentioned previously, the ebullition cycle consists of two distinct phases, with a single period being the sum of the growth and wait times, and the frequency being equal to the inverse of that period, as shown in Eq. 2.1. For reasons similar to that of the nucleation site density, it has been difficult to create a mechanistic model for the bubble departure frequency over an entire surface, with early correlations instead focusing on the relationship between frequency and bubble diameter, since it follows to reason that both the rate of bubble growth as well as size at departure determine the duration of the growth phase. However, these models seem to neglect the weight of the dwell phase, which is particularly pronounced at low heat fluxes.

The first study by Jakob and Fitz (1931) proposed a simple relationship between the bubble departure frequency and bubble diameter:

$$f_b = 0.078 \left(\frac{1}{D_b} \right) \tag{4.8}$$

Zuber (1963) decided on a relationship between bubble release and natural convection to arrive at the following correlation:

$$f_b = \frac{1}{D_b} \left(0.59 \left[\frac{\sigma g (\rho_l - \rho_g)}{\rho_l^2} \right]^{1/4} \right) \tag{4.9}$$

Cole (1960) using the following in the inertia controlled region:

$$f_b = \left(\frac{1}{D_b} \frac{4}{3} \left[\frac{g(\rho_l - \rho_g)}{C_d \rho_l} \right] \right)^{1/2}$$

(4.10)

where C_d is the drag coefficient and equal to 1 for water at 1atm.

These three models for the frequency are plotted in Figure 4.2 as a function of bubble diameter.For comparison against heat flux, which is how the experimental data was collected, I have also plotted these three models as a function of heat flux by using the Jensen and Memmel (1986) model for bubble diameter, as seen in 4.3.
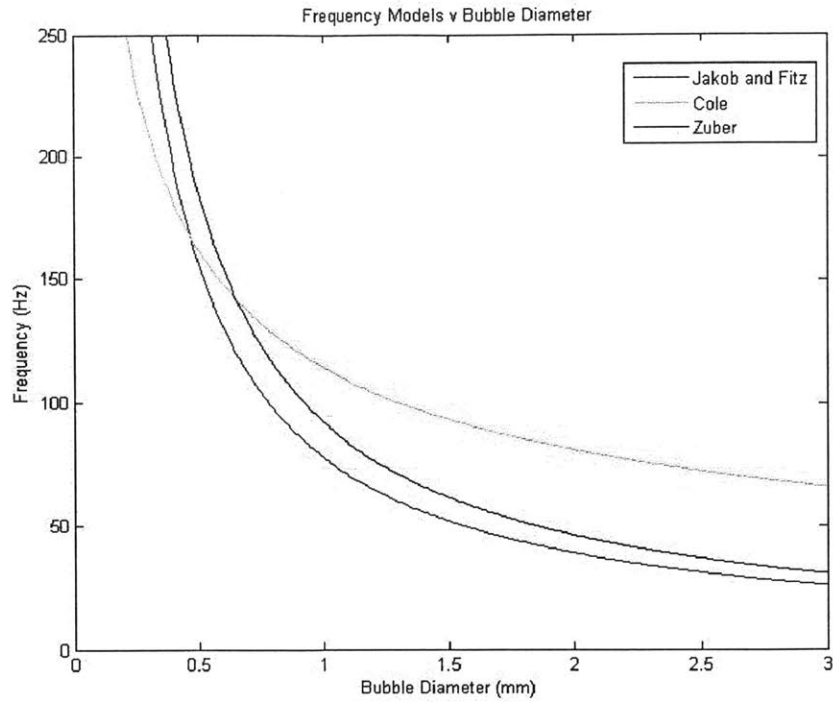
Figure 4.2: Frequency models as a function of bubble diameter for saturated water at atmospheric temperature
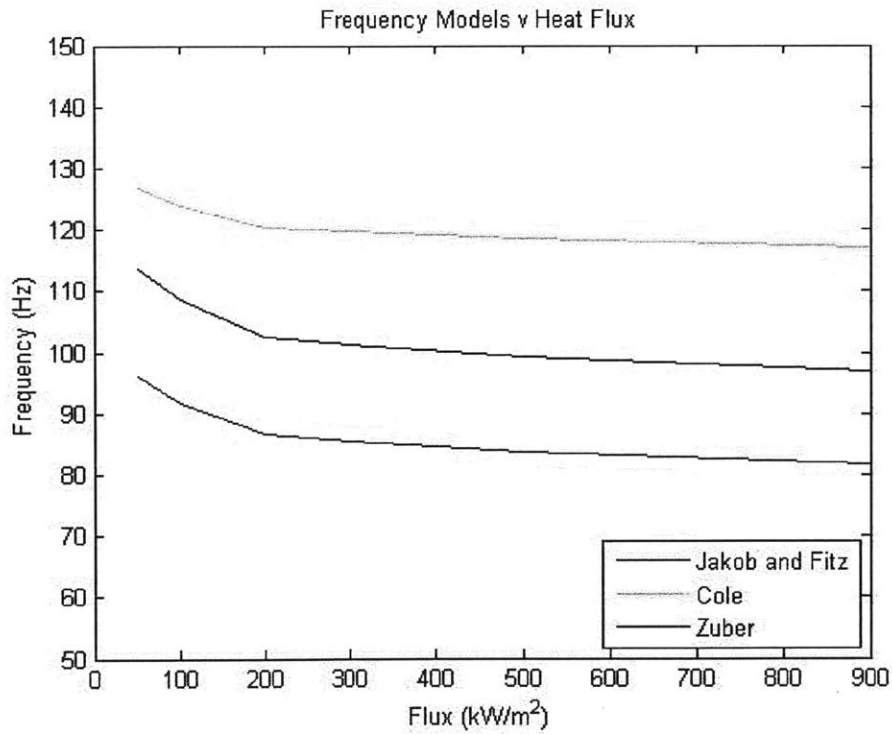

Figure 4.3: The frequency models plotted against heat flux by using the Jensen and Memmel correlation for bubble

diameter for saturated water and atmospheric pressure.

4.3.1 Mechanistic Models for the Ebullition Cycle

As the focus of this work, I choose to take a closer look at the ebullition cycle and nucleation frequency, taking the basic principles approach offered by Podowski's theoretically rigorous, mechanistic models, as outlined in his 1997 and 2008 papers. After going through the thermodynamic balance equations, Podowski comes to a series of equations that define the temperature profile and duration of the dwell and growth phases of the ebullition cycle. The first of these equations is for $T_i(0+)$, which is the temperature at which the dwell phase begins:

$$T_i(0^+) = \left(\frac{k_w T_0}{\sqrt{a_w}} + \frac{k_l T_{bl}}{\sqrt{a_l}}\right) * \left(\frac{k_w}{\sqrt{a_w}} + \frac{k_l}{\sqrt{a_l}}\right)^{-1} \tag{4.11}$$

Where T_{bl}, is the bulk temperature at a distance corresponding to the laminar sublayer thickness, and T_0 is the average temperature of the nucleation site. The formulation for T_0 can be seen below:

$$T_0 = \frac{1}{\theta_D + \theta_G} \int_0^{\theta_D + \theta_G} T(t) dt \tag{4.12}$$

Where T(t) during the dwell period is:

$$T_i(t) = T_i(0^+) + \frac{2 * \dot{q}_H}{\sqrt{\pi} * \left(\frac{k_w}{\sqrt{a_w}} + \frac{k_l}{\sqrt{a_l}}\right)} * \sqrt{t} \quad for \ 0 \leq t \leq \Theta_D \tag{4.13}$$

And T(t) during the growth period can be modeled as dropping linearly from $T_i(\Theta_D)$ to $T_i(0+)$:

$$T_i(t) = T_i(\theta_D) - \left(\frac{T_i(\theta_D) - T_i(0^+)}{\theta_G}\right) * t \quad for \ \Theta_D < t \leq \Theta_G \tag{4.14}$$

Θ_D is the time of transition from the dwell to the growth period, and this shift occurs when the bubble radius becomes equal to the cavity radius r_c. Using the Clausius-Clapeyron equation, and

21

knowing that at this instant the temperature on either side of the hemispherical bubble must be

equal, Podowski arrives at the following relationship

$$T_{sat} + \frac{2\sigma T_{sat} v_{fg}}{r_c h_{fg}} = T_i(\theta_D) - \frac{(T_i(0^+) - T_{bl})r_c}{\sqrt{\pi \alpha_l \theta_D}} - \frac{B k_w r_c}{R \sqrt{\pi \alpha_l}} \qquad (4.15)$$

where

$$B = \frac{q''}{k_w}$$

$$R = \frac{k_w}{\sqrt{\pi \alpha_w}} + \frac{k_l}{\sqrt{\pi \alpha_l}}$$

As can be seen, for given wall properties, fluid properties, and thermal conditions, Eq. (4.15)

reduces to a quadratic equation for the dwell time Θ_D. Podowski reaches an analogous

expression for the growth time Θ_G, which is seen in Eq.(4.16) below, where D_b is the bubble

diameter at departure:

$$\frac{D_b \rho_g h_{fg}}{2 k_w} = -B \theta_G + \frac{2(T_{sat} - T_i(\theta_D))}{\sqrt{\pi a_w}} \sqrt{\theta_G} \qquad (4.16)$$

If the dwell time is known, the average surface heat flux during the dwell period can be

determined using the above expression by integrating from 0 to Θ_D, where Θ_D is the length of the

dwell time:

$$|q_D''| = \frac{2 * k_l * [T_i(0^+) - T_{bl}]}{\sqrt{\pi a_l \theta_D}} + \frac{q_H'}{1 + \frac{k_w}{k_l} \sqrt{\frac{a_l}{a_w}}} \qquad (4.17)$$

22

There is an analogous equation for the average surface heat flux during the growth period which also integrates the expression for the growth time, and needs both the dwell period time (with $T(\Theta_D)$) and also the growth time Θ_G as inputs:

$$\left|\dot{q_G}\right| = \frac{1}{\theta_G} \int_{\theta_D}^{\theta_D + \theta_G} \left|q_w''\right| dt = q_H'' + 2k_w \frac{T_i(\Theta_D) - T_{bl}}{\sqrt{\pi a_w \Theta_G}} \qquad (4.18)$$

Finally, the equation that ties all of these together states that the total heat flux times the period time is equal to the product of the average dwell period flux and growth period flux with their respective times, as shown here:

$$\left|q_G''\right| * \Theta_G + \left|q_D''\right| * \Theta_D = q_H''(\Theta_D + \Theta_G) \qquad (4.19)$$

At the end of all this, we are left with a set of unknowns: Θ_D, Θ_G, $\dot{q_G}''$, q_D'', T_o, and the corresponding equations of 4.15, 4.16, 4.17, 4.18, and 4.12 to solve for them.

5. Comparison of Models against Experimental Data

For the experimental values, I decided to base much of the comparison on the 08_006 run for DI Water. This set of data was typical with respect to other DI runs, and therefore considered a good basis for comparison. Figure 5.1 shows the comparison of selected models with the measured bubble diameter.
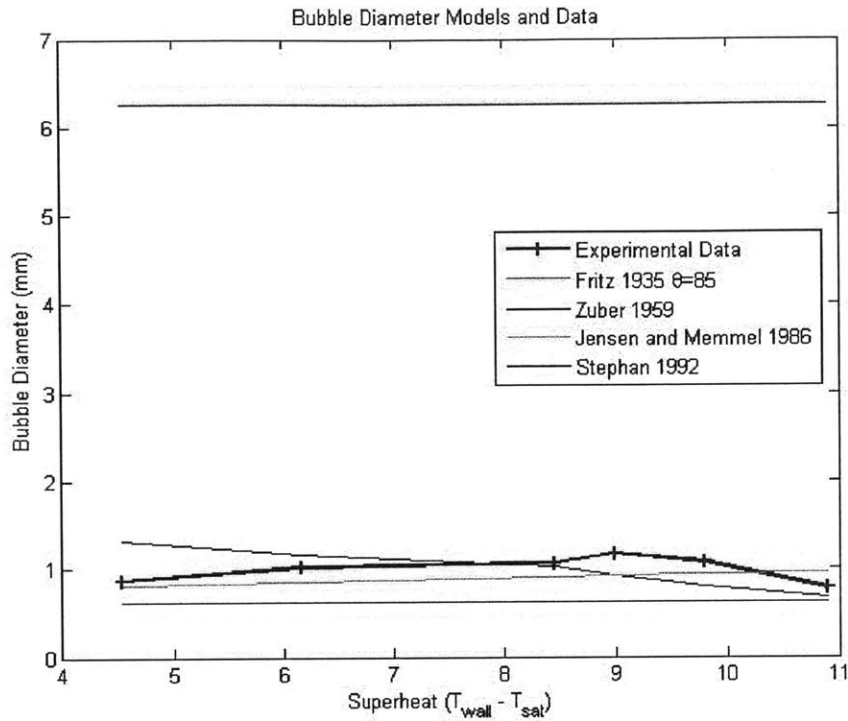
Figure 5.1. Bubble diameter models with experimental data superimposed.

It can be seen that the oldest model (Fritz) over predicts the measured values many times over. However, most of the other models seem to correspond well, especially considering that the error of the measured diameter is on the order of ±20%.

Figure 5.2 shows the model and data for the nucleation site density. The values used for the model in Eq. 4.7 were 1500 for K and 8/3 for m.
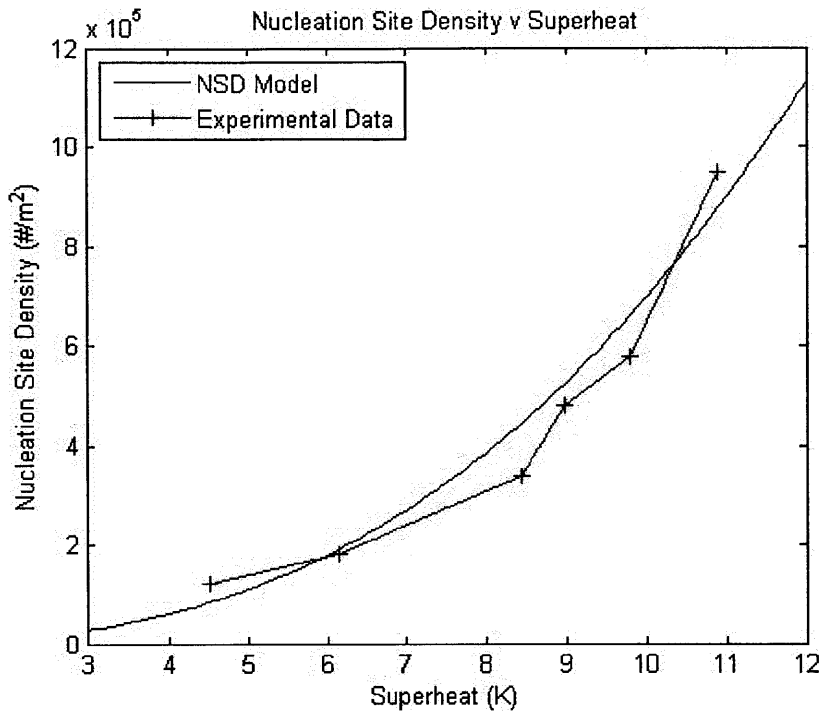
Figure 5.2: Experimental and model nucleation site density v wall superheat. 1500 and 8/3 were chosen for K and m, respectively

What can be observed from the lines in Figure 5.2 is that the NSD model can be made to fit the data reasonably well for specific values of the coefficients K and m.

5.1 Models and Data for Ebullition Cycle

The first approach of this work in considering the various equations for the ebullition model put forth by Podowski was to take several of the parameters directly from the data of multiple experimental runs, and see how the remaining models fit with the experiment when given true values.

5.1.1 Data from the 08_004 Run at 50kW/m^2

Table 5.1 shows the averaged values for T_o, the dwell time, and the growth time, which were all pulled from this particular experimental data set, and then put into the models that needed them.

Table 5.1: Data pulled from experiment 08_004 at 50 kW/m^2	
Parameter	**Experimental Value**
T_o	109.18 C
dwell time	0.1029 s
growth time	0.0076 s

Using the information from the experimental data and plugging them into the corresponding

models, the models produced the values found in Table 5.2. The value selected for T_{bl} was of

102C, which was considered to be a good approximation, but it was not rigorously investigated.

Table 5.2: Outputs of the models using data from Table 5.1	
Model For:	**Output Value**
T(0+)	108.12 C
q"(growth)	1,019,000 W/m^2
q"(dwell)	42,950 W/m^2
frequency (1/t_{total})	9.078 Hz
q" from heater	107,800 W/m^2

Figure 5.3 shows the experimental ebullitions cycles that were selected from a specific site over

multiple periods, and also has superimposed on it the model's predictions, using the values from

the experimental data in Table 5.1 as inputs and with the curvature during the dwell time

expressed by Eq. (4.13).
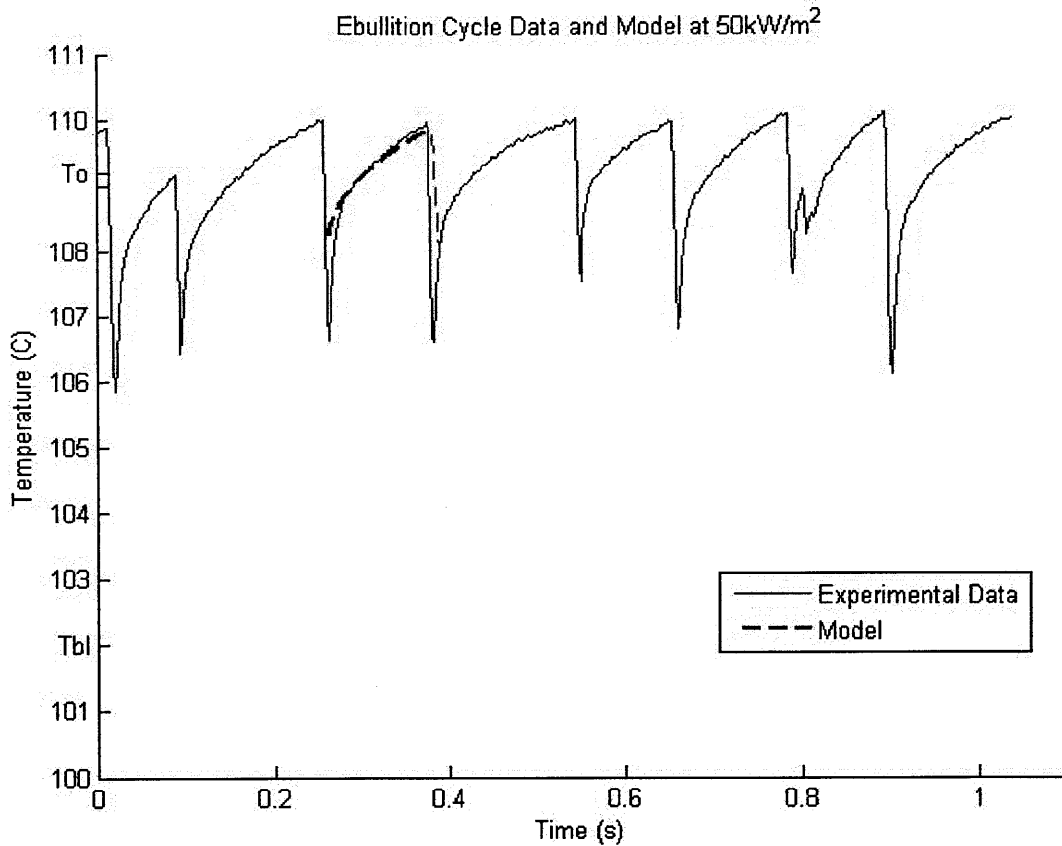
Figure 5.3: The temperature response graph from the experiment set for 08_004 at 50kW/m^2, with the model

predictions for curvature superimposed over a single period.

Observations

Some things to be noted from this figure is that the model seems to fit rather well over the data,

however, each period is slightly different, due to the randomness of this process, so it is not

always going to coincide as well as it did in this particular example.

Also, the predicted value of T(0+) is at least 1 degree higher than the actual temperature at which the dwell phase begins. Since almost all of the ebullition models use T(0+) as a parameter, this has implications across all of the predicted values. It will affect Θ_D since it will take less time to restore the boundary layer equilibrium after a bubble has departed, and that change in Θ_D will go on to affect the average surface heat flux during the dwell and growth periods. However, just in terms of matching the data, it can be seen that trying to force T(0+) to correspond with the experimental value (essentially a vertical shift downward) would make the data lose its overall agreement, since the values at all points would end up being lower than the experimental values, and the peak temperature in particular would be much lower.

Finally, it is not surprising that the predicted heater flux value is higher than the average heat flux of 50 kW/m^2, since all of these models specifically consider the nucleation site and ebullition cycle, which has greater temperature gradients than the areas outside the influence of bubble growth i.e. where there is only convective heat transfer.

5.1.2 Data from 08_004 Run at 250 kW/m^2 and at 500 kW/m^2

To gain more accurate insight, multiple data sets were compared against the model's predictions. Following the same process as for the data set above, the experimental values for the 08_004 run at 250 kW/m^2 were gathered and put in to Table 5.3.

Table 5.3: Data pulled from experiment 08_004 at 250 kW/m^2	
Parameter	Experimental Value
T$_o$	108.11 C
dwell time	0.0321 s
growth time	0.0041 s

Using the experimental data from Table 5.3, the model's predictions can be seen in Table 5.4.

Table 5.4: Outputs of the models using data from Table 5.1	
Model For:	Output Value
T(0+)	108.12 C
q"(growth)	1,883,000 W/m^2
q"(dwell)	91,050 W/m^2
frequency (1/t$_{total}$)	27.6 Hz
q" from heater	294,000 W/m^2

Using the predictions from Table 5.4, and with the dwell time curvature predicted by Eq.(xz),

Figure 5.4 was produced, showing the experimental data along with the model ebullition cycle

superimposed over the data.
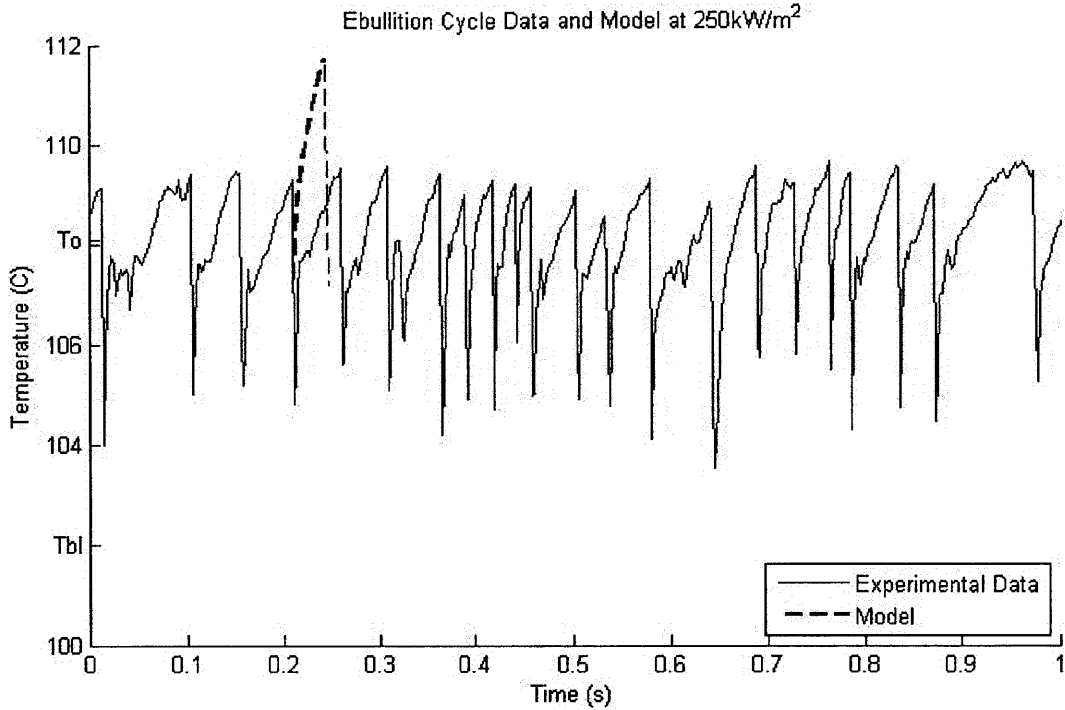
Figure 5.4: Data and model for the 08_004 run at 250 kW/m^2.

The same process as above was used for a heat flux of 500 kW/m^2. Table 5.5 contains the collected averages for the run with a heat flux of 500 kW/m^2.

Table 5.5: Data pulled from experiment 08_004 at 500 kW/m^2	
Parameter	Experimental Value
T_o	114.06 C
dwell time	0.0138 s
growth time	0.0032 s

Plugging the numbers from Table 5.5 into the models results in the outputs seen in Table 5.6.

Table 5.6: Outputs of the models using data from Table 5.5	
Model For:	**Output Value**
T(0+)	112.28 C
q"(growth)	3,147,000 W/m^2
q"(dwell)	200,680 W/m^2
frequency $(1/t_{total})$	58.82 Hz
q" from heater	755,270 W/m^2

Figure 5.5 shows the results of the models with these parameters superimposed over the data set.
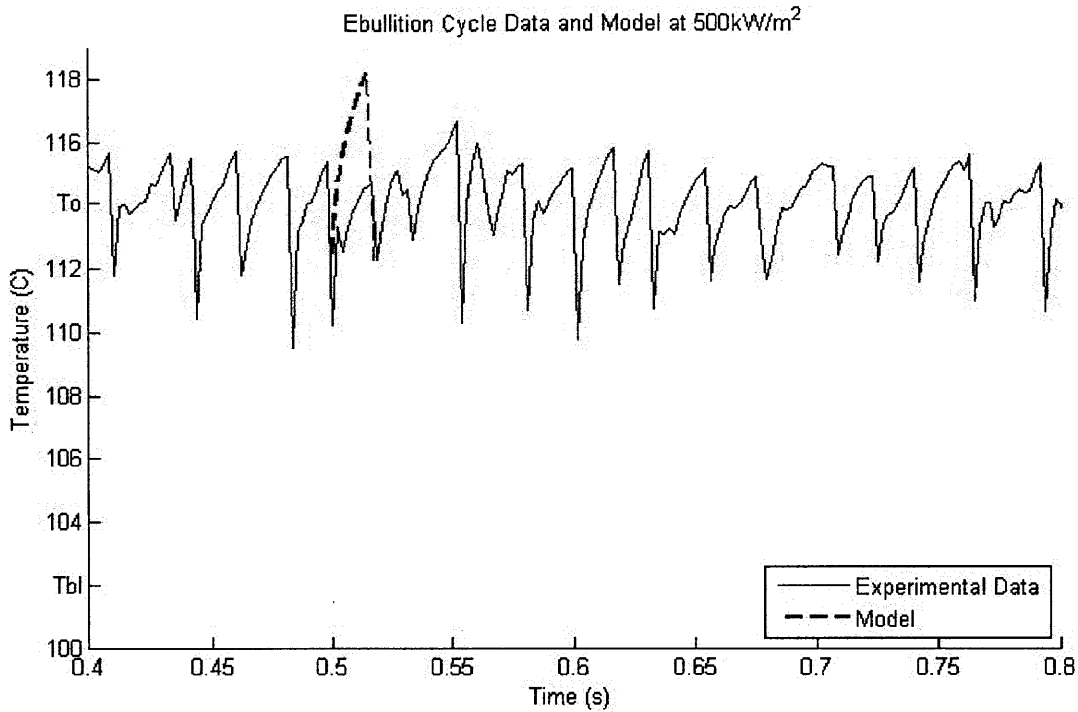
Figure 5.5: Data and model for the 08_004 run with a heat flux of 500kW/m^2.

Observations

There are a couple of significant points which can be observed from the runs at 250 kW and 500 kW. What jumps out immediately is that the values predicted by the models are at a much higher temperature than what was see in the experiments. An interesting divergence here from the 50 kW data set is that if T(0+) for the models were to actually correspond to the temperature at which the dwell phase begins in the experiments, then they would be very good approximations. This is exemplified in Figure 5.6, where T(0+) was set to 105 C for the 250 kW data set.
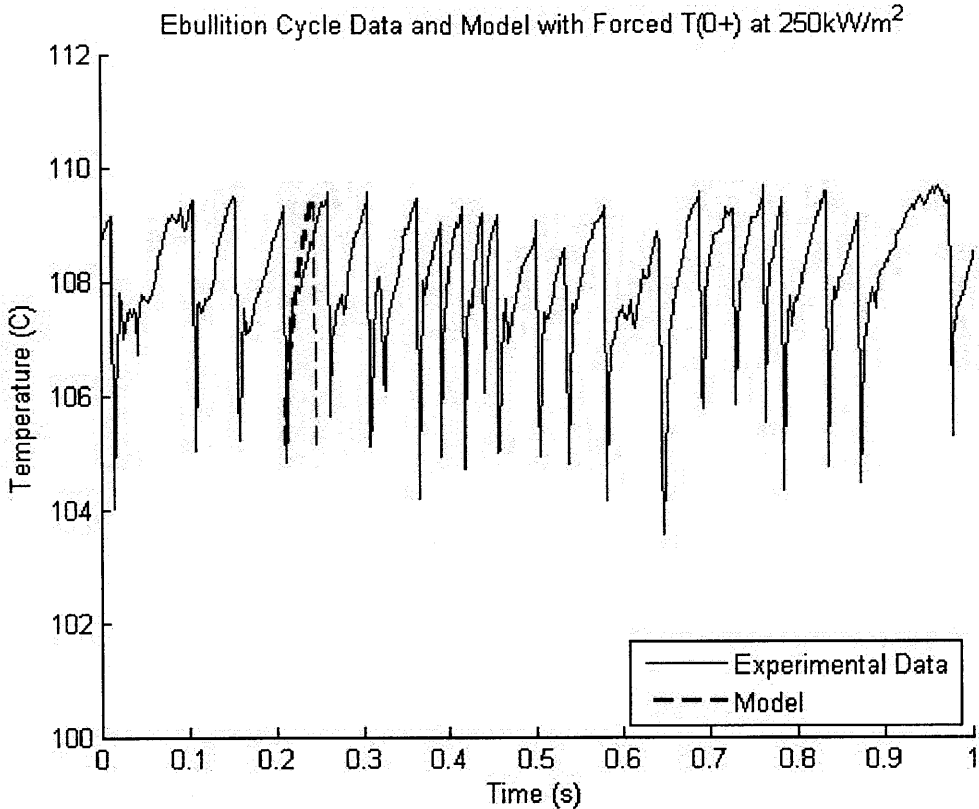
Figure 5.6: The results of setting T(0+) at the experimental value of 105 C, and how the model corresponds with the data with that specific parameter being pulled from the experimental data.

The result seen in Figure 5.6 shows that if a proper starting point is selected, the model for $T_i(t)$ corresponds remarkably well with the experimental data. This validation of Eq. (4.13) for the curvature of the dwell phase, given the right conditions, is a significant observation, and shows that the underlying principles in deriving the behavior during the dwell phase were correct and seems to be reflected in the experimental data.

Other points of note are that there are certain trends which can be inferred from these three data points. The frequency does increase with increasing heat flux, and the root of this seems to be from the drastic drop in the duration of the dwell period Θ_D, since the growth time stays

33

relatively close across all the experiments, especially considering that the maximum absolute error in those measurements is 4 ms.

Another point is interest is that the later two data sets, for 250 and 500 kW, better reflect the degree of randomness involved in the nucleation process, which often erratic behavior in the temperature response. This could be a result of such things as measurement error in not capturing the growth phases, the influence from surrounding bubbles, etc. The first data set, shown in Figure 5.3, actually seems to be somewhat out of the norm in its behavior. This could be due to the low heat flux allowing for more time for the process to follow its course smoothly, and also factors such as the cavity radius, which itself can have a large impact on the duration of the growth and dwell periods, and also on the superheat necessary to begin nucleation.

The higher value of q_h at the nucleation site over average q_h from the heater in general is also seen to continue, though to varying orders greater. There are very wide swings in this heat flux value, going from tens of thousands during the dwell phase to millions of kW/m^2 during the growth phase.

5.1.3 Sensitivity Analysis

In order to verify how strongly uncertainty or variability of the parameters affected the values predicted by the models, some of the parameters for the 08_004 50 kW data were modified and then run through the models again. The differences in the predicted values were tabulated, with both the new value and the percent change from the original predictions. These results can be seen in Table 5.7.

Table 5.7: Results of sensitivity tests to modification of various parameters.

Modification	T(0+) Celsius	q"(growth) W/m^2	q"(dwell) W/m^2	frequency	q"(heater)
growth time +10%	*	9.74e5 (-4.4%)	*	8.987(-1%)	1.133e5(+5.1%)
growth time +20%	*	9.35e5 (-8.27%)	*	8.92(-1.6%)	1.1592e5(+7%)
growth time -10%	*	1.072e6(+5.16%)	*	9.1125(*)	1.074e5(-0.3%)
growth time -20%	*	1.133e6(+11.24%)	*	9.1764(+1.1%)	1.01e5(-6.65%)
T_bl +0.5 C	108.1981 (+0.078 C)	9.667e5 (-5.1%)	4.0475e4 (-5.76%)	*	1.045e5 (-3%)
T_bl +1 C	108.272 (+0.152 C)	9.1432e5 (-10.3%)	3.800e4 (-11.5%)	*	9.856e4 (-8.55%)
T_bl -0.5 C	108.0504 (-0.07 C)	1.0716e6 (+5.16%)	4.542e5 (+5.76%)	*	1.164e5(+7.94%)
dwell time +10%	*	1.0287e6 (+0.96%)	4.1295e4 (-3.85%)	8.2788 (-8.8%)	1.0374e5 (-3.76%)
dwell time +20%	*	1.0388e6 (+1.94%)	3.9851e4 (-7.21%)	7.6291 (-16%)	9.8066e4 (-9%)
dwell time -10%	*	1e6 (-1.16%)	4.4874e4 (+4.5%)	9.9783 (+9.9%)	1.1823e5 (+9.67%)
dwell time -20%	*	9.955e5 (-2.3%)	4.715e4 (+9.77%)	11.12 (+22.5%)	1.277e5 (+18.47%)

It can be seen that the difference in value ranges from negligible to 10+%. It is also significant that selecting an appropriate T_{bl} is non-trivial, since just a one degree difference results in about a 10% change in the predicted values of the heat flux. Furthermore, since the maximum absolute error in the growth and dwell time measurements was 4ms, and the average growth period was only 7.6ms, the ±20% to the growth times is a very likely range to exist, and should be taken into consideration for further study. Error of 20% for the dwell time is unlikely at these low heat flux levels, but becomes more of a possibility at higher heat fluxes, since the dwell time drops exponentially with increasing heat flux.

In general, the change in predicted values is in or below the 10% range; and if the models can be found to match the data reasonably well, then a 10% error from any one parameter would still be a very good approximation.

6. Conclusion

There is still much can be learned and interpreted from the vast amount of data which was collected. Brief analysis showed that there is potential for good agreement with experimental results and some of the models and empirical correlations for the bubble diameter and nucleation site density. In looking into the ebullition models proposed by M.Z. Podowski, good agreement was found with the predicted curvature and shape of the ebullition cycle, although the disagreement in T(0+) became a legitimate issue which needs further investigation. For future work, I would recommend attempting to base the dwell and growth times from the models rather than pulling them directly from the experiment, and seeing how well the predicted times match the averages for the growth and wait times of the individual nucleation sites. If those models could be validated and found to be in high agreement, then the nucleation frequency parameter itself would have a basic principles approach for solving.

References

1. C.D. GERARDI, "Investigation of the Pool Boiling Heat Transfer Enhancement of Nano-Engineered Fluids by means of High-Speed Infrared Thermography", PhD Thesis, MIT, Department of Nuclear Engineering (May 2009)

2. M.Z. PODOWSKI "Recent Developments in the Modeling of Boiling Heat Transfer Mechanisms", Keynote paper N14P1444, Proc. NURETH-13 Kanazawa City, Japan, 2009.

3. M.Z. PODOWSKI, R.M. PODOWSKI, "Mechanistic Multidimensional Model of Forced Convection Boiling Heat Transfer", *Science and Technology of Nuclear Installations*, 387020 (2009).

4. R.M. PODOWSKI, D.A. DREW, R.T. LAHEY, M.Z. PODOWSKI, "A Mechanistic Model of the Ebullition Cycle in Forced Convection Subcooled Boiling", *Eighth Int. Topl. Mtg. on Nuclear Reactor Thermal-Hydraulics*, Kyoto, Japan, September 30-October 4, 1997.